Utah State University

DigitalCommons@USU

Space Dynamics Lab Publications | Space Dynamics Lab

1-1-2014

Spin-Assisted Angles-Only Navigation and Control For SmallSats

Randy Christensen

David Geller

Follow this and additional works at: https://digitalcommons.usu.edu/sdl_pubs

Recommended Citation

Christensen, Randy and Geller, David, "Spin-Assisted Angles-Only Navigation and Control For SmallSats" (2014). *Space Dynamics Lab Publications.* Paper 30.
https://digitalcommons.usu.edu/sdl_pubs/30

This Article is brought to you for free and open access by the Space Dynamics Lab at DigitalCommons@USU. It has been accepted for inclusion in Space Dynamics Lab Publications by an authorized administrator of DigitalCommons@USU. For more information, please contact digitalcommons@usu.edu.

Christensen, Randy, and David Geller. 2014. "Spin-Assisted Angles-Only Navigation and Control for Smallsats." Paper presented at the 37th Annual AAS Guidance and Control Conference, Breckenridge, CO, Jan. 31–Feb. 5.

(Preprint) AAS 14-067

SPIN-ASSISTED ANGLES-ONLY NAVIGATION AND CONTROL FOR SMALLSATS

Randy Christensen[*], **David Geller**[†]

This work analyzes the ability to estimate and control the relative position and velocity of a Small Satellite with respect to a target vehicle using a single optical camera. Although the target range is generally unobservable when using angles-only measurements, relative position/velocity observability can be achieved when the SmallSat is slowly rotating and the camera is offset from the center of gravity. The sensitivity of the navigation errors and trajectory dispersions to several simulation parameters is discussed, including SmallSat camera offset, spin rate, and range to target. Also included in the analysis is the effect of common sensor errors (e.g. camera and gyro bias/noise), external disturbances, and initial conditions. Future efforts are mentioned to extend the analysis to cooperative/uncooperative targets and to increase analysis efficiency through Linear Covariance analysis.

INTRODUCTION

The practice of single camera optical-based angles-only relative navigation represents a low-cost, low-power, and low-mass/volume solution to the orbital relative navigation problem.[1,2] However, it suffers from a well known range observability problem.[3] I.e. the relative position/velocity state is not observable during orbital proximity operations when angles-only measurements and Clohessy-Wiltshire dynamics are employed.[4]

Some useful theoretical observability research has been conducted,[5,6] wherein two practical approaches have been suggested to overcome this range observability problem. In the first approach, a nominal or special translational maneuver is executed to help determine the unknown range parameter.[7,8,9] Such translational maneuvers however require additional propellant and increase satellite ΔV requirements. In the second approach, knowledge of target spacecraft size, shape, or location of known features is used to determine the unknown range parameter. This however requires a priori information about the target spacecraft.[10]

Recently, a solution to the range observability problem that does not require translational maneuvers nor a priori knowledge of target spacecraft geometry was demonstrated.[11] The proposed solution employs small vehicle rotational maneuvers and a camera center-of-mass offset in the formulation of the estimation problem. For the purposes of this paper, this method is named Spin-Assisted Angles-Only Navigation.

The objective of this paper is to explore the trade space associated with Spin-Assisted Angles-Only Navigation, to determine achievable estimation accuracies with realistic hardware and error

[*]Senior Mechanical Engineer, C4ISR Division, Space Dynamics Laboratory, 1695 Research Park Way, North Logan, UT 84341.

[†]Associate Professor, Mechanical and Aerospace Engineering, Utah State University, 4130 Old Main Hill Logan, UT 84322.

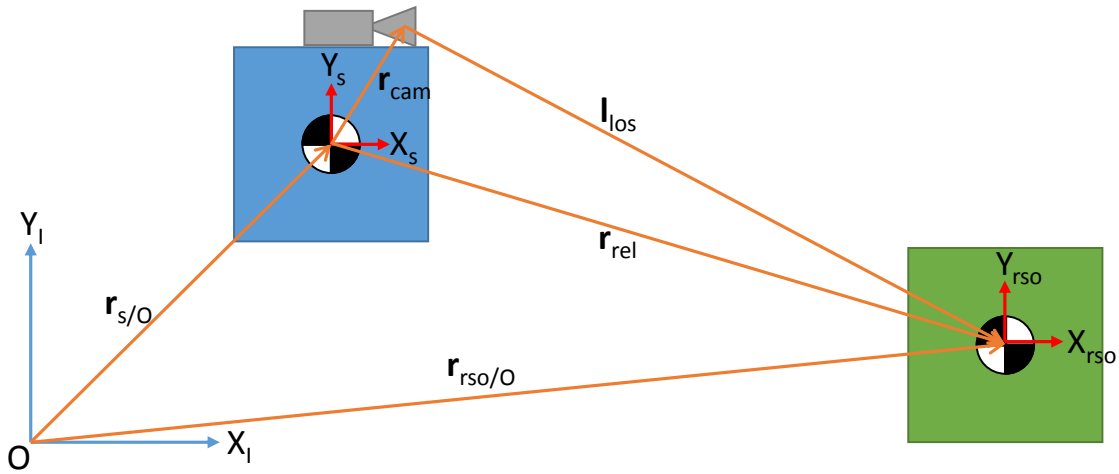

Figure 1. Satellite Geometry

sources. Following the problem formulation, a trade study is performed to identify key parameters and trends related to range estimation accuracy. Following the trade space analysis, a rendezvous mission will be designed and analyzed. The ability of the navigation filter to calculate accurate range estimation errors will be assessed via Monte Carlo analysis. Also through Monte Carlo analysis, the rendezvous accuracy will be assessed by calculating the position dispersions along the trajectory.

PROBLEM FORMULATION

Figure 1 illustrates the geometry of the SmallSat and the Resident Space Object (RSO) being analyzed. The SmallSat is equipped with gyros to sense angular rates and a star camera to measure attitude. In addition, the SmallSat contains a line-of-sight (LOS) camera offset from its center of gravity (CG). The LOS camera (shown on top of the SmallSat) is used to track the location of the RSO CG. The SmallSat also employs acceleration and torque actuators to control position and attitude. The RSO, however, is assumed to be a dead and uncooperative satellite. Specifically, it contains neither actuators for position/attitude control, nor communication equipment to provide information to the SmallSat. Disturbance torques and accelerations operate on both satellites. The objective of the SmallSat is to autonomously estimate its position relative to the RSO, then execute position commands to approach the RSO.

The remainder of this section defines the mathematical models of the system described previously. It is split into four subsections. The Truth Models subsection describes the truth state vector and its associated dynamics and driving noise. It also defines the measurement models for each of the sensors on-board the SmallSat. The Navigation subsection outlines the state/covariance propagation and update equations of the angles-only extended Kalman filter. The Position and Attitude Control subsection defines the control law for the position and attitude controllers. Finally, the Simulation Parameters subsection defines several important quantities needed for the simulation.

Truth Models

The truth state vector is partitioned into four sets of states

$$\boldsymbol{x} = \begin{bmatrix} \boldsymbol{x}_s^T & \boldsymbol{x}_{rso}^T & \boldsymbol{x}_p^T & \boldsymbol{x}_f^T \end{bmatrix}_{37\times1}^T \tag{1}$$

The SmallSat and RSO states, $\boldsymbol{x}_s$ and $\boldsymbol{x}_{rso}$, contain the inertial position, velocity, attitude quaternion, and angular rate of each vehicle. The parameter state vector, $\boldsymbol{x}_p$ contains the biases of the gyro, LOS camera, and star camera. Finally, the feature vector $\boldsymbol{x}_f$ contains the location of the feature being observed by the LOS camera. For the purposes of this paper, the feature is the CG of the RSO. Thus $\boldsymbol{r}^{rso}$ is nominally zero, but with some uncertainty as will be defined later.

$$\boldsymbol{x}_s = \begin{bmatrix} \boldsymbol{r}_{s/O}^I \\ \boldsymbol{v}_{s/O}^I \\ \boldsymbol{q}_I^S \\ \boldsymbol{\omega}_{s/I}^s \end{bmatrix}_{13\times1} \quad \boldsymbol{x}_{rso} = \begin{bmatrix} \boldsymbol{r}_{rso/O}^I \\ \boldsymbol{v}_{rso/O}^I \\ \boldsymbol{q}_I^{rso} \\ \boldsymbol{\omega}_{rso/I}^{rso} \end{bmatrix}_{13\times1} \quad \boldsymbol{x}_p = \begin{bmatrix} \boldsymbol{b}_{gyro} \\ \boldsymbol{b}_{los} \\ \boldsymbol{b}_{star} \end{bmatrix}_{8\times1} \quad \boldsymbol{x}_f = \begin{bmatrix} \boldsymbol{r}^{rso} \end{bmatrix}_{3\times1} \tag{2}$$

The truth state dynamics are defined as a non-linear function of the state, $\boldsymbol{x}$, and actuator command, $\hat{\boldsymbol{u}}$, with additive white Gaussian noise $\boldsymbol{w}$

$$\dot{\boldsymbol{x}} = \boldsymbol{f}\left(\boldsymbol{x}, \hat{\boldsymbol{u}}\right) + B\boldsymbol{w} \qquad E\left[\boldsymbol{w}\left(t\right)\boldsymbol{w}^T\left(t'\right)\right] = S_w\delta\left(t - t'\right) \tag{3}$$

The detailed equations for $\boldsymbol{f}\left(\boldsymbol{x}, \hat{\boldsymbol{u}}\right)$, B, and S_w of Equation (3) are included in the appendix. Suffice it to say that the position and velocity states of both spacecraft are modeled with rectilinear motion, a good approximation for the motion between two spacecraft in close proximity. The attitude and angular rate states are modeled with quaternion kinematics and Euler's equation. The parameter states are modeled as first-order Markov processes. Finally, the feature location is modeled as constant in time.

The actuator command vector $\hat{\boldsymbol{u}}$ comprises command accelerations and torques to control the position and orientation of the SmallSat. The process noise vector $\boldsymbol{w}$ captures the effects of disturbance accelerations and torques on both spacecraft as well as the random nature of the sensor biases.

$$\hat{\boldsymbol{u}} = \begin{bmatrix} \boldsymbol{a}_{com}^I \\ \boldsymbol{M}_{com}^s \end{bmatrix}_{6\times1} \qquad \boldsymbol{w} = \begin{bmatrix} \boldsymbol{a}_{s,dist}^I \\ \boldsymbol{M}_{s,dist}^s \\ \boldsymbol{a}_{rso,dist}^I \\ \boldsymbol{M}_{rso,dist}^{rso} \\ \boldsymbol{w}_{b,gyro} \\ \boldsymbol{w}_{b,los} \\ \boldsymbol{w}_{b,star} \end{bmatrix}_{20\times1} \tag{4}$$

The measurements available to the SmallSat consist of angular rate data provided by a 3-axis gyro, attitude quaternion provided by the star camera, and LOS measurements to the RSO CG provided by the LOS camera, all of which are corrupted by bias and noise. The gyro, star camera, and LOS camera measurement models are shown in Equations (5), (6), and (7), respective

$$\tilde{\boldsymbol{\omega}}_{s/I}^s = \boldsymbol{\omega}_{s/I}^s + \boldsymbol{b}_{gyro} + \boldsymbol{n}_{gyro} \quad E\left[\boldsymbol{n}_{gyro}\left(t\right)\boldsymbol{n}_{gyro}^T\left(t'\right)\right] = I_{3\times3}\sigma_{n,gyro}^2\delta\left(t - t'\right) \tag{5}$$

$$\tilde{\boldsymbol{z}}_{star} = \tilde{\boldsymbol{q}}_I^s = \begin{pmatrix} \frac{1}{2}(\boldsymbol{b}_{star} + \boldsymbol{\epsilon}_{star}) \\ 1 \end{pmatrix} \otimes \boldsymbol{q}_I^s, \quad E\left[\boldsymbol{\epsilon}_{star,k}\boldsymbol{\epsilon}_{star,k'}\right] = I_{3\times3}\sigma_{n,star}^2\delta_{kk'} \tag{6}$$

$$\tilde{\boldsymbol{z}}_{los} = \begin{bmatrix} l_z/l_x \\ l_y/l_x \end{bmatrix} + \boldsymbol{b}_{los} + \boldsymbol{\nu}_{los}, \quad E\left[\boldsymbol{\nu}_{los,k}\boldsymbol{\nu}_{los,k'}\right] = I_{3\times3}\sigma_{n,los}^2\delta_{kk'} \tag{7}$$

where the line-of-sight vector is further defined using the position, orientation, LOS camera offset, and RSO CG location.

$$\boldsymbol{l}_{los}^s = \begin{pmatrix} l_x \\ l_y \\ l_z \end{pmatrix} \qquad \boldsymbol{l}_{los}^s = \left(T_I^s \boldsymbol{r}_{rso/O}^I + T_I^s T_{rso}^I \boldsymbol{r}^{rso}\right) - \left(T_I^s \boldsymbol{r}_{s/O}^I + \boldsymbol{r}_{cam}^s\right) \tag{8}$$

Navigation

A formal derivation of the angles-only extended Kalman filter requires the definition of a "design model", followed by linearization of both the dynamics and measurement equations about the current state estimate. This derivation is beyond the scope of this work. Therefore, only the final result is listed here. As in the case of the truth state vector, the navigation state vector is partitioned into four sets of states

$$\hat{\boldsymbol{x}} = \begin{bmatrix} \hat{\boldsymbol{x}}_s^T & \hat{\boldsymbol{x}}_{rso}^T & \hat{\boldsymbol{x}}_p^T & \hat{\boldsymbol{x}}_f^T \end{bmatrix}^T \tag{9}$$

The SmallSat state vector contains the relative position, velocity, and inertial attitude of the SmallSat. The RSO state vector contains the inertial attitude, angular rate, and angular acceleration of the RSO. The parameter state vector contains the bias for the gyros, navigation camera , and star camera on-board the SmallSat. Finally, the feature state vector accounts for the nominally zero location of the RSO center of gravity.

$$\hat{\boldsymbol{x}}_s = \begin{bmatrix} \hat{\boldsymbol{r}}_{rel}^I \\ \hat{\boldsymbol{v}}_{rel}^I \\ \boldsymbol{q}_I^{\hat{s}} \end{bmatrix}_{10\times1} \quad \hat{\boldsymbol{x}}_{rso} = \begin{bmatrix} \boldsymbol{q}_I^{r\hat{s}o} \\ \hat{\boldsymbol{\omega}}_{rso/I}^{rso} \\ \hat{\boldsymbol{\alpha}}_{rso/I}^{rso} \end{bmatrix}_{10\times1} \quad \hat{\boldsymbol{x}}_p = \begin{bmatrix} \hat{\boldsymbol{b}}_{gyro} \\ \hat{\boldsymbol{b}}_{los} \\ \hat{\boldsymbol{b}}_{star} \end{bmatrix}_{8\times1} \quad \hat{\boldsymbol{x}}_f = \begin{bmatrix} \hat{\boldsymbol{r}}^{rso} \end{bmatrix}_{3\times1} \tag{10}$$

The propagation of the navigation state is a non-linear function of the state estimate, commanded acceleration, and gyro measurements

$$\dot{\hat{\boldsymbol{x}}} = \hat{\boldsymbol{f}}\left(\hat{\boldsymbol{x}}, \boldsymbol{a}_{com}^I, \tilde{\boldsymbol{\omega}}_{s/I}^s\right) \tag{11}$$

The details of Equation (11) are included in the appendix. The relative position and velocity states are modeled with rectilinear motion. The SmallSat attitude is propagated with "model replacement" using gyro measurements.[12] Since the SmallSat has no knowledge of the inertia matrix nor the disturbance torques acting on the RSO, it propagates the attitude and angular rate using an first-order Markov angular acceleration model. The sensor parameters and RSO CG location are modeled as in the truth state dynamics.

The covariance propagation is derived by defining an "error state vector", $\delta\boldsymbol{x}$, which in all states except for the quaternion states is defined as the difference between the estimated state and the true state, $\boldsymbol{x} = \hat{\boldsymbol{x}} + \delta\boldsymbol{x}$. The quaternion error states are defined as a small rotation from the true quaternion, i.e. $\boldsymbol{q}_I^s = \begin{bmatrix} \frac{\delta\boldsymbol{\theta}_s}{2} \\ 1 \end{bmatrix} \otimes \boldsymbol{q}_I^{\hat{s}}$ and $\boldsymbol{q}_I^{rso} = \begin{bmatrix} \frac{\delta\boldsymbol{\theta}_{rso}}{2} \\ 1 \end{bmatrix} \otimes \boldsymbol{q}_I^{r\hat{s}o}$. The covariance of this error state

vector is propagated using the following equation where, the matrices $\hat{F}$, $\hat{B}$, $\hat{S}_w$ are defined in the appendix.

$$\dot{\hat{P}} = \hat{F}\hat{P} + \hat{P}\hat{F}^T + \hat{B}\hat{S}_w\hat{B}^T \tag{12}$$

The update portion of the extended Kalman filter comprises two steps: 1) Estimation of the error state vector, 2) Application of the estimated error state to the navigation state/covariance.[13] In the case of both measurements, the error state vector is estimated by multiplying the Kalman gain by the residual, $\delta\boldsymbol{z}$.

$$\delta\hat{\boldsymbol{x}}^+ = \hat{K}_k\delta\boldsymbol{z} \tag{13}$$

In the case of the LOS measurements, the residual is simply the difference between the measured and the predicted LOS measurement, $\tilde{\boldsymbol{z}}_{los} - \hat{\tilde{\boldsymbol{z}}}_{los}$. The attitude residual, $\delta\tilde{\boldsymbol{\theta}}_s$, however is defined via quaternion multiplication

$$\tilde{\boldsymbol{q}}_I^s \otimes \boldsymbol{q}_{\hat{s}}^I \otimes \begin{bmatrix} \frac{-\hat{\boldsymbol{b}}_{star}}{2} \\ 1 \end{bmatrix} = \begin{bmatrix} \frac{\delta\tilde{\boldsymbol{\theta}}_s}{2} \\ 1 \end{bmatrix} \tag{14}$$

The Kalman gain is defined as

$$\hat{K}_k = \hat{P}_k^- \hat{H}_k^T \left(\hat{H}_k\hat{P}_k^-\hat{H}_k^T + \hat{R}_\nu\right)^{-1} \tag{15}$$

Where the measurement noise matrix $\hat{R}_\nu$ corresponds to the measurement being processed. The measurement geometry matrix, $\hat{H}_k$, also depends on the measurement being processed, and is listed in the following equations for the star camera and LOS camera measurements

$$H_{star} = \begin{bmatrix} 0_{3\times6} & I_{3\times3} & 0_{3\times14} & I_{3\times3} & 0_{3\times3} \end{bmatrix} \tag{16}$$

$$\hat{H}_{los} = \hat{H}_l\hat{H}_x + \hat{H}_{exp} \tag{17}$$

where

$$\hat{H}_l = \begin{bmatrix} -\hat{l}_z/\hat{l}_x^2 & 0 & 1/\hat{l}_x \\ -\hat{l}_y/\hat{l}_x^2 & 1/\hat{l}_x & 0 \end{bmatrix} \tag{18}$$

$$\hat{H}_x = \begin{bmatrix} T_I^{\hat{s}} & 0_{3\times3} & \left[\left(T_I^{\hat{s}}\hat{\boldsymbol{r}}_{rel}^I + T_I^{\hat{s}}T_{r\hat{s}o}^I\hat{\boldsymbol{r}}^{rso}\right)\times\right] & -T_I^{\hat{s}}T_{r\hat{s}o}^I\left[\hat{\boldsymbol{r}}^{rso}\times\right] & 0_{3\times14} & T_I^{\hat{s}}T_{r\hat{s}o}^I \end{bmatrix} \tag{19}$$

$$\hat{H}_{exp} = \begin{bmatrix} 0_{2\times21} & I_{2\times2} & 0_{2\times3} & 0_{2\times3} \end{bmatrix} \tag{20}$$

Once the the error state vector is estimated, both the state and covariance values are updated. For all but the quaternion states, the update is simply the old state plus the estimated error, $\hat{\boldsymbol{x}}_c = \hat{\boldsymbol{x}} + \delta\hat{\boldsymbol{x}}^+$. The quaternions, however are updated via quaternion multiplication, $\left(\boldsymbol{q}_I^{\hat{s}}\right)_c = \begin{bmatrix} \frac{\delta\boldsymbol{\theta}_s}{2} \\ 1 \end{bmatrix}^+ \otimes \boldsymbol{q}_I^{\hat{s}}$ and $\left(\boldsymbol{q}_I^{r\hat{s}o}\right)_c = \begin{bmatrix} \frac{\delta\boldsymbol{\theta}_s}{2} \\ 1 \end{bmatrix}^+ \otimes \boldsymbol{q}_I^{r\hat{s}o}$. Finally the covariance is updated using the following.

$$\hat{P}_k^+ = \left(I - \hat{K}_k\hat{H}_k\right)\hat{P}_k^-\left(I - \hat{K}_k\hat{H}_k\right)^T + \hat{K}_k\hat{R}_\nu\hat{K}_k^T \tag{21}$$

Table 1. Disturbance Parameters 3σ

Symbol	Value	Units	Description
$S_{a,s}$	0.0	m^2/s^3	SmallSat Disturbance Acceleration PSD
$S_{a,rso}$	variable	m^2/s^3	RSO Disturbance Acceleration PSD
$S_{m,s}$	$(1\exp -6)^2$	N^2m^2s	SmallSat Disturbance Torques PSD
$S_{m,rso}$	$(1\exp -4)^2$	N^2m^2s	RSO Disturbance Torques PSD
$\sigma_{\alpha,ss}$	$1\exp -7$	rad/s^2	Steady-state RSO angular acceleration uncertainty
τ_α	60	s	RSO angular acceleration first-order Markov time constant

Table 2. Sensor Parameters 3σ

Symbol	Value	Units	Description
$\sigma_{b,gyro,ss}$	variable	$deg/hour$	Steady-state gyro bias uncertainty
$\sigma_{b,los,ss}$	variable	$mrad$	Steady-state LOS camera bias uncertainty
$\sigma_{b,star,ss}$	variable	$mrad$	Steady-state star camera bias uncertainty
τ_{gyro}	12	hr	Gyro bias first-order Markov time constant
τ_{los}	12	hr	LOS camera bias first-order Markov time constant
τ_{star}	12	hr	Star camera bias first-order Markov time constant
$\sigma_{n,gyro}$	variable	$deg/\sqrt{hr}$	Gyro angular random walk
$\sigma_{n,los}$	variable	$mrad$	LOS camera measurement noise
$\sigma_{n,star}$	variable	$mrad$	Star camera measurement noise

Position and Attitude Control

The command acceleration and torques are computed using a proportional + derivative control law

$$\hat{\boldsymbol{u}} = \begin{bmatrix} \boldsymbol{a}^I_{com} \\ \boldsymbol{M}^s_{com} \end{bmatrix} = \begin{bmatrix} K_r(\hat{\boldsymbol{r}}^I_{rel} - \boldsymbol{r}^I_{desired}) + K_v(\hat{\boldsymbol{v}}^I_{rel} - \boldsymbol{v}^I_{desired}) \\ K_\theta(\Delta\hat{\boldsymbol{\theta}}^s_{com}) + K_\omega(\hat{\boldsymbol{\omega}}^s_{s/I} - \boldsymbol{\omega}^s_{desired}) \end{bmatrix} \tag{22}$$

where the angular error is extracted from the quaternion product, $\boldsymbol{q}_{desired} \otimes \hat{\boldsymbol{q}}^{s*}_I = \begin{pmatrix} \frac{1}{2}\Delta\hat{\boldsymbol{\theta}}^s_{com} \\ 1 \end{pmatrix}$.

Simulation Parameters

Tables 1 through 4 list several important parameters related to the simulation. In the case that a parameter is varied during the subsequent trade study, the value is denoted as "variable". The disturbance sources are listed in Table 1. SmallSat sensor parameters are listed in Table 2. The controller parameters and inertia matrices are listed in Table 3 Finally, the truth state uncertainties listed in Table 4 are used to initialize the truth state and navigation states.

Table 3. Controller and Physical Parameters

Symbol	Value	Units	Description
K_r	$I_{3\times3}\omega_n^2$	$1/s^2$	Position controller proportional gain
K_v	$I_{3\times3}2\zeta\omega_n$	$1/s$	Position controller derivative gain
K_θ	$\omega_n^2 J_s$	$N \cdot m/rad$	Attitude controller proportional gain
K_ω	$2\zeta\omega_n J_s$	$N \cdot m \cdot s/rad$	Attitude controller derivative gain
ω_n	$2\pi 0.05$	rad/s	Position and attitude controller natural frequency
ζ	1	NA	Position and attitude controller damping ratio
J_s	$diag\left(\begin{bmatrix} 33 & 83 & 83 \end{bmatrix}\right)$	$kg \cdot m^2$	SmallSat inertia matrix
J_{rso}	$diag\left(\begin{bmatrix} 25 & 30 & 30 \end{bmatrix}\right)$	$kg \cdot m^2$	RSO inertia matrix

Table 4. Truth State Initial Uncertainty 3σ

Symbol	Value	Units	Description
$\sigma_{r,s}$	0	m	SmallSat position
$\sigma_{v,s}$	0	m/s	SmallSat velocity
$\sigma_{\theta,s}$	$\sqrt{\sigma_{b,star,ss}^2 + \sigma_{n,star}^2}$	$mrad$	SmallSat attitude
$\sigma_{\omega,s}$	7	$\mu rad/s$	SmallSat angular rate
$\sigma_{r,rso}$	$5r_0$	m	RSO position
$\sigma_{v,rso}$	0.01	m/s	RSO velocity
$\sigma_{\theta,rso}$	0	$mrad$	RSO attitude
$\sigma_{\omega,rso}$	100	$\mu rad/s$	RSO angular rate
$\sigma_{b,gyro}$	$\sigma_{b,gyro,ss}$	$deg/hour$	Gyro bias
$\sigma_{b,los}$	$\sigma_{b,los,ss}$	$mrad$	LOS camera bias
$\sigma_{b,star}$	$\sigma_{b,star,ss}$	$mrad$	Star camera bias
σ_α	$\sigma_{\alpha,ss}$	rad/s^2	RSO angular acceleration
σ_r	1	mm	RSO CG location
r_0	variable	m	Initial SmallSat range

Table 5. Range Estimation Trade Space

Sensor Suite	Noisy RSO	Quiet RSO
Low Cost Sensors	1	4
Moderate Cost Sensors	2	5
High Cost Sensors	3	6

Table 6. Sensor Suite Parameters

Sensor Parameter	Low Cost	Moderate Cost	High Cost
$\sigma_{b,star,ss}\,(mrad)$	10.0	1.0	0.1
$\sigma_{n,star}\,(mrad)$	10.0	1.0	0.1
$\sigma_{b,gyro,ss}\,(deg/hr)$	10.0	1.0	0.1
$\sigma_{n,gyro}\left(deg/\sqrt{hr}\right)$	0.7	0.07	0.007
$\sigma_{b,los,ss}\,(mrad)$	10	1	0.1
$\sigma_{n,los}\,(mrad)$	10	1	0.1

RANGE ESTIMATION TRADE STUDY

The trade space studied in this paper is illustrated in table 5, and spans a range of sensor accuracies. Table 6 lists the specs for a low cost, moderate cost, and high cost navigation sensor suite. Table 7 lists the RSO acceleration noise PSD, with the associated translational uncertainty at 100 seconds.

Figures 2 to 4 illustrate the steady-state standard deviation of the range estimation errors for each element of the trade space. The range errors are plotted as a function of the SmallSat spin rate. The quiet RSO is shown on the left, with the noisy RSO on the right. To investigate the sensitivity of the estimation errors to range and the LOS camera offset, curves for lever arms of 0.1, 0.5, and 1.0 meters are shown at two ranges, 10m and 50m. The Low-Cost hardware at a range of 50 meters is omitted due to the unrealistically-long convergence time of the filter, making it an impractical choice both from a simulation time standpoint and practical system standpoint.

Several important observations can be taken from the trade study analysis. One of the more trivial observations is that increased RSO translational noise increases the range estimation errors. This is due to the unknown drift of the RSO between LOS camera measurements. The translational

Table 7. RSO Translational Noise

RSO Parameter (3σ)	Noise RSO	Quiet RSO
Translational Uncertainty (m @100 sec)	1.0	0.1
$S_{a,rso}\left(m^2/s^3\right)$	$(0.0017)^2$	$(0.00017)^2$

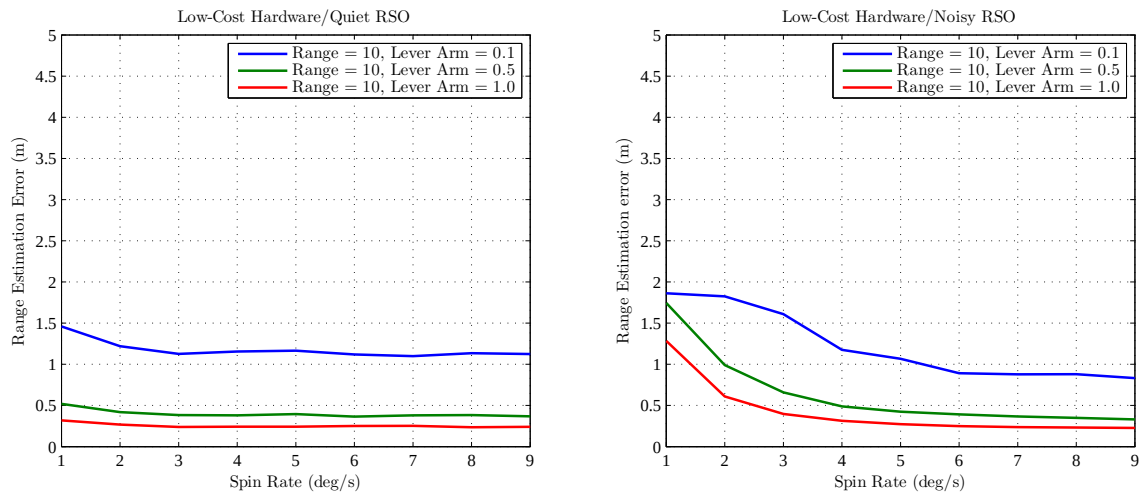

Figure 2. Low Cost Sensor Range Estimation 1σ

noise however can be overcome by increasing the spin rate. This is most clearly illustrated when comparing the left plot to the right plot. In most cases, the noisy RSO estimation errors converge to the quiet RSO errors, for a given set of hardware, range, and LOS camera offset.

Another important observation is that, for a given configuration, there exists a spin rate above which no improvement is made in estimation errors. In a real-world application, it is important to identify this threshold, so as to not require a spin rate higher than is necessary. This is important because high spin rates can degrade the accuracy of other sensors on-board, e.g. the star camera.

The last observation made is related to the sensitivity of estimation errors to the distance between the SmallSat and RSO. With increasing distance to the RSO comes increased range errors. The influence of distance can also be overcome by increasing the LOS camera offset. This creates a greater angular separation between LOS measurements, resulting in a more accurate estimate of range.

ANGLES-ONLY RENDEZVOUS MISSION DESIGN AND ANALYSIS

This section analyzes the navigation and control performance of a specific angles-only rendezvous mission. The objective for the SmallSat is to approach a quiet RSO at constant velocity, from a distance of 50m to 2m in 10 minutes. The moderate cost sensor suite with a LOS camera offset of 0.5m was selected to achieve centimeter-level range estimates inside 10 meters distance. A spin rate of 3 degrees/second was selected to be near the flat region of range estimation vs. spin rate curve, without spinning faster than is necessary.

The metrics used in the analysis are divided into two groups: relative position estimation errors and relative position dispersions. The metrics were computed using Monte Carlo analysis with 200 runs. Figure 5 illustrates the performance of the navigation filter in estimating the range, horizontal, and vertical positions of the SmallSat using "hair plots". The true estimation errors for each individual run are shown in light gray. The 3σ standard deviation of the 200 runs is shown in blue, with 95% confidence intervals shown in dashed red. The navigation filter's estimate of the 3σ standard deviations is shown in teal. While the cross track estimation errors converge quickly, the range

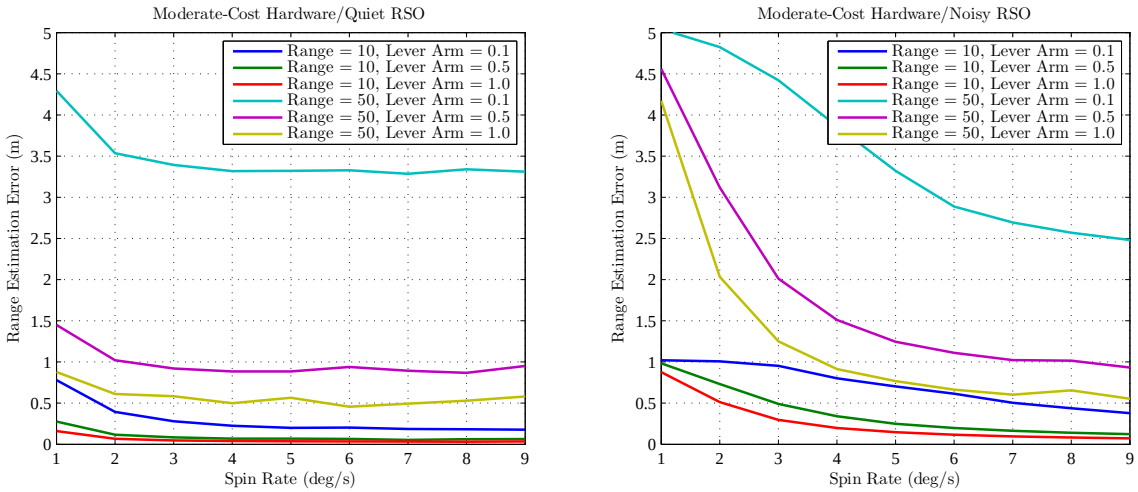

Figure 3. Moderate Cost Sensor Range Estimation 1σ

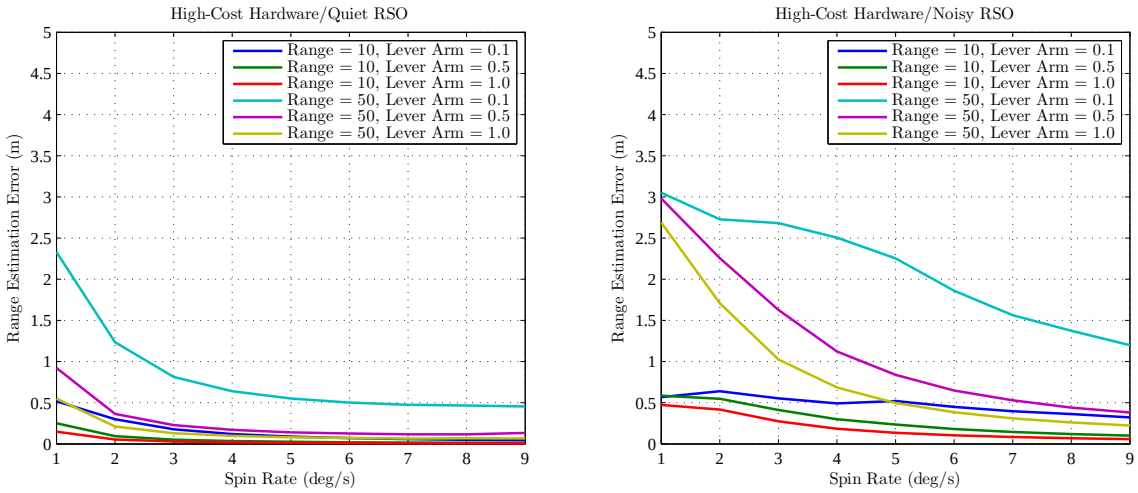

Figure 4. High Cost Sensor Range Estimation 1σ

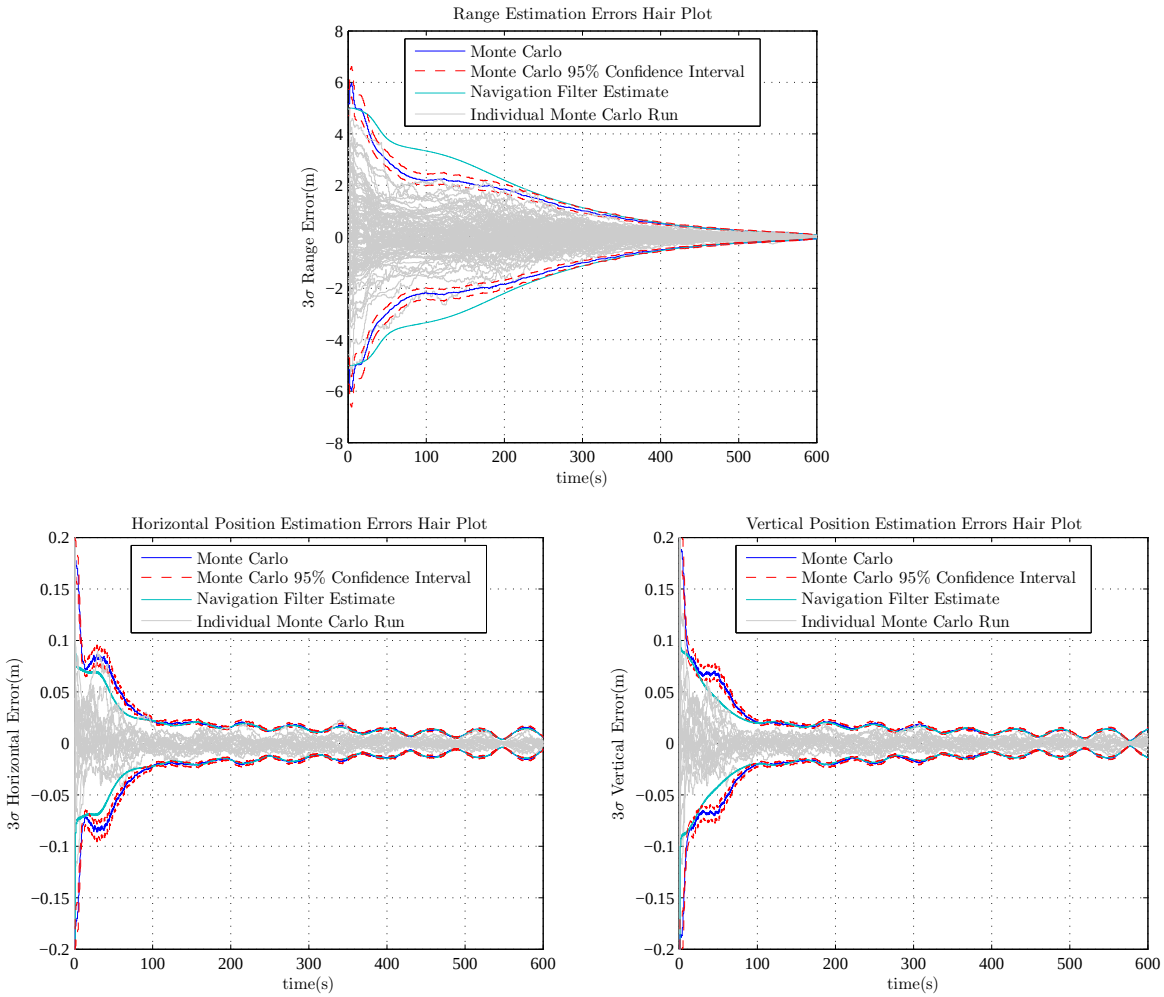

Figure 5. Navigation Filter Estimation Accuracy

errors take much longer, reducing almost linearly with time/range to the target. There exists a small period of time at the beginning of the trajectory where filter's estimate of the errors is slightly inaccurate. In the case of the range errors, the filter is initially conservative (i.e. the estimate error is larger than the true error). In both cross track errors, however, the filter is initially optimistic. After the initial transient, the filter accurately estimates the errors for both range and cross-track directions, even capturing the fluctuations present in the cross track errors, happening twice per rotation of the SmallSat (or a period of 60 seconds). The source of this oscillation is currently unknown.

Figure 6 shows the true relative position dispersions as a function of range to the RSO. As expected, the position dispersions follow the same trends as the navigation errors, namely relatively slow convergence of range dispersions, and relatively fast convergence of cross track dispersions. In addition, the cross track dispersions exhibit the same ringing behavior observed in the estimation errors. The final position dispersions are 9cm in range and less than 2cm in the cross track dimensions.

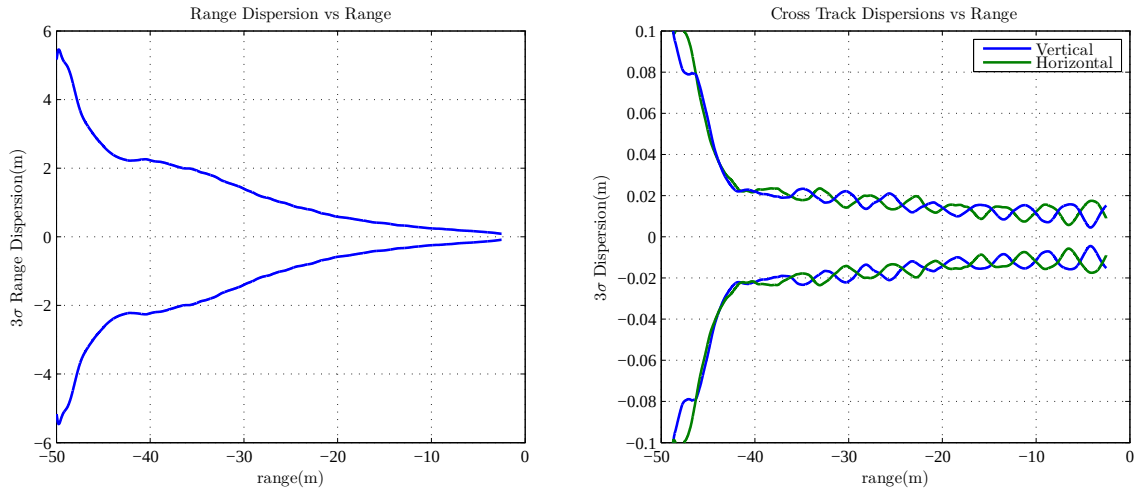

Figure 6. Relative Position Dispersions

CONCLUSIONS

The trade space associated with Spin-Assisted Angles-Only Navigation was explored. The sensitivity of range estimation errors to navigation sensor accuracies, SmallSat spin rate, RSO translational noise, LOS camera offsets, and range was determined. It was found that much of the adverse affects related to range and RSO translational noise can be overcome by increasing spin rate and LOS camera offsets. The trade space analysis was used as the basis for an angles-only rendezvous mission design. The Monte Carlo analysis of this mission illustrated the ability of the navigation filter to accurately estimate position errors. The final position dispersions for this mission were 9cm in range and less than 2cm in the cross track dimensions

Future work comprises extending Spin-Assisted Angles-Only Navigation to cooperative targets with multiple features at known locations, and uncooperative targets with unknown feature locations. In addition, a Linear Covariance model is being developed to enable rapid simulations and trade studies.

NOTATION

Position and velocity vectors are denoted with the letter $\boldsymbol{r}$ and $\boldsymbol{v}$. Subscripts of position and velocity vectors denote the origin and the coordinate system upon which it is projected. For example $\boldsymbol{v}^I_{rso/O}$ represents the velocity of the RSO with respect to the origin, projected onto I frame coordinates. Attitude quaternions are represented with the symbol $\boldsymbol{q}^s_I$ which corresponds to the rotation matrix T^s_Ithat transforms a vector from the the I frame to the s frame. The angular rate of a vehicle is represented with the symbol $\boldsymbol{\omega}$ with subscripts and superscripts. For example $\boldsymbol{\omega}^s_{s/I}$ represents the angular rate of the s frame with respect to the I frame, projected onto s frame axes. A variable adorned with a $\hat{()}$ represents a quantity estimated by the Kalman filter. For example $\hat{\boldsymbol{r}}_{rel}$ is the Kalman filter's estimate of the relative position. A variable adorned with a $\tilde{()}$ represents the measurement of a physical quantity corrupted by noise sources. Finally, sensor biases are represented with the letter $\boldsymbol{b}$ and a subscript denoting to which sensor it belongs.

APPENDIX: TRUTH AND NAVIGATION STATE DYNAMICS DETAILED EQUATIONS

$$\boldsymbol{f}\left(\boldsymbol{x},\hat{\boldsymbol{u}}\right)=\begin{bmatrix} \boldsymbol{v}^{I}_{s/O} \\ \boldsymbol{a}^{I}_{com} \\ \frac{1}{2}\begin{pmatrix} \boldsymbol{\omega}^{s}_{s/I} \\ 0 \end{pmatrix}\otimes \boldsymbol{q}^{s}_{I} \\ J_s^{-1}(-\boldsymbol{\omega}^{s}_{s/I}\times J_s\boldsymbol{\omega}^{s}_{s/I}+\boldsymbol{M}^{s}_{com}) \\ \boldsymbol{v}^{I}_{rso/O} \\ 0_{3\times1} \\ \frac{1}{2}\begin{pmatrix} \boldsymbol{\omega}^{rso}_{rso/I} \\ 0 \end{pmatrix}\otimes \boldsymbol{q}^{rso}_{I} \\ J_{rso}^{-1}(-\boldsymbol{\omega}^{rso}_{rso/I}\times J_{rso}\boldsymbol{\omega}^{rso}_{rso/I}) \\ -\frac{\boldsymbol{b}_{gyro}}{\tau_{gyro}} \\ -\frac{\boldsymbol{b}_{los}}{\tau_{los}} \\ -\frac{\boldsymbol{b}_{star}}{\tau_{star}} \\ 0_{3\times1} \end{bmatrix}_{36\times1} \tag{23}$$

$$S_w = diag\left(S_{a,s}, S_{m,s}, S_{a,rso}, S_{m.rso}, \frac{2\sigma^2_{gyro}}{\tau_{gyro}}I_{3\times3}, \frac{2\sigma^2_{los}}{\tau_{los}}I_{2\times2}, \frac{2\sigma^2_{star}}{\tau_{star}}I_{3\times3}\right)_{20\times20} \tag{24}$$

$$B=\begin{bmatrix} 0_{3\times3} & 0_{3\times3} & 0_{3\times3} & 0_{3\times3} & 0_{3\times3} & 0_{3\times2} & 0_{3\times3} \\ I_{3\times3} & 0_{3\times3} & 0_{3\times3} & 0_{3\times3} & 0_{3\times3} & 0_{3\times2} & 0_{3\times3} \\ 0_{4\times3} & 0_{4\times3} & 0_{4\times3} & 0_{4\times3} & 0_{4\times3} & 0_{4\times2} & 0_{4\times3} \\ 0_{3\times3} & J_s^{-1} & 0_{3\times3} & 0_{3\times3} & 0_{3\times3} & 0_{3\times2} & 0_{3\times3} \\ 0_{3\times3} & 0_{3\times3} & 0_{3\times3} & 0_{3\times3} & 0_{3\times3} & 0_{3\times2} & 0_{3\times3} \\ 0_{3\times3} & 0_{3\times3} & I_{3\times3} & 0_{3\times3} & 0_{3\times3} & 0_{3\times2} & 0_{3\times3} \\ 0_{4\times3} & 0_{4\times3} & 0_{4\times3} & 0_{4\times3} & 0_{4\times3} & 0_{4\times2} & 0_{4\times3} \\ 0_{3\times3} & 0_{3\times3} & 0_{3\times3} & J_{rso}^{-1} & 0_{3\times3} & 0_{3\times2} & 0_{3\times3} \\ 0_{3\times3} & 0_{3\times3} & 0_{3\times3} & 0_{3\times3} & I_{3\times3} & 0_{3\times2} & 0_{3\times3} \\ 0_{2\times3} & 0_{2\times3} & 0_{2\times3} & 0_{2\times3} & 0_{2\times3} & I_{2\times2} & 0_{2\times3} \\ 0_{3\times3} & 0_{3\times3} & 0_{3\times3} & 0_{3\times3} & 0_{3\times3} & 0_{3\times2} & I_{3\times3} \\ 0_{3\times3} & 0_{3\times3} & 0_{3\times3} & 0_{3\times3} & 0_{3\times3} & 0_{3\times2} & 0_{3\times3} \end{bmatrix} \tag{25}$$

$$\boldsymbol{f}\left(\boldsymbol{x},\hat{\boldsymbol{u}}\right)=\begin{bmatrix} \hat{\boldsymbol{v}}_{rel}^{I} \\ -\boldsymbol{a}_{com}^{I} \\ \frac{1}{2}\begin{bmatrix} \tilde{\boldsymbol{\omega}}_{s/I}^{s}-\hat{\boldsymbol{b}}_{gyro} \\ 0 \end{bmatrix}\otimes \boldsymbol{q}_{I}^{\hat{s}} \\ \frac{1}{2}\begin{bmatrix} \hat{\boldsymbol{\omega}}_{rso/I}^{rso} \\ 0 \end{bmatrix}\otimes \boldsymbol{q}_{I}^{\hat{rso}} \\ \hat{\boldsymbol{\alpha}}_{rso/I}^{rso} \\ -\frac{1}{\tau_{\alpha}}\hat{\boldsymbol{\alpha}}_{rso/I}^{rso} \\ -\frac{1}{\tau_{gyro}}\hat{\boldsymbol{b}}_{gyro} \\ -\frac{1}{\tau_{los}}\hat{\boldsymbol{b}}_{los} \\ -\frac{1}{\tau_{star}}\hat{\boldsymbol{b}}_{star} \\ 0_{3\times 1} \end{bmatrix}_{31\times 1} \tag{26}$$

$$\hat{F}=\begin{bmatrix} \hat{F}_{s1} & 0_{9\times 9} & \hat{F}_{s2} & 0_{9\times 3N_f} \\ 0_{9\times 9} & \hat{F}_{rso} & 0_{9\times 8} & 0_{9\times 3N_f} \\ 0_{8\times 9} & 0_{8\times 9} & \hat{F}_{p} & 0_{8\times 3N_f} \\ 0_{3N_f\times 9} & 0_{3N_f\times 9} & 0_{3N_f\times 8} & 0_{3N_f\times 3N_f} \end{bmatrix} \tag{27}$$

$$\hat{F}_{s1}=\begin{bmatrix} 0_{3\times 3} & I_{3\times 3} & 0_{3\times 3} \\ 0_{3\times 3} & 0_{3\times 3} & 0_{3\times 3} \\ 0_{3\times 3} & 0_{3\times 3} & -\left(\tilde{\boldsymbol{\omega}}_{s/I}^{s}-\hat{\boldsymbol{b}}_{gyro}\right)\times \end{bmatrix} \tag{28}$$

$$\hat{F}_{s2}=\begin{bmatrix} 0_{3\times 3} & 0_{3\times 2} & 0_{3\times 3} \\ 0_{3\times 3} & 0_{3\times 2} & 0_{3\times 3} \\ -I_{3\times 3} & 0_{3\times 2} & 0_{3\times 3} \end{bmatrix} \tag{29}$$

$$\hat{F}_{rso}=\begin{bmatrix} -\left(\hat{\boldsymbol{\omega}}_{rso/I}^{rso}\right)\times & I_{3\times 3} & 0_{3\times 3} \\ 0_{3\times 3} & 0_{3\times 3} & I_{3\times 3} \\ 0_{3\times 3} & 0_{3\times 3} & -1/\tau_{\alpha}I_{3\times 3} \end{bmatrix} \tag{30}$$

$$\hat{F}_{p}=\begin{bmatrix} -1/\tau_{gyro}I_{3\times 3} & 0_{3\times 2} & 0_{3\times 3} \\ 0_{2\times 3} & -1/\tau_{los}I_{2\times 2} & 0_{2\times 3} \\ 0_{3\times 3} & 0_{3\times 2} & -1/\tau_{star}I_{3\times 3} \end{bmatrix} \tag{31}$$

$$\hat{B}=\begin{bmatrix} \hat{B}_{1} & 0_{15\times 11} \\ 0_{11\times 6} & I_{11\times 11} \\ 0_{3N_f\times 6} & 0_{3N_f\times 11} \end{bmatrix} \tag{32}$$

$$\hat{B}_{1}=\begin{bmatrix} 0_{3\times 3} & 0_{3\times 3} \\ I_{3\times 3} & 0_{3\times 3} \\ 0_{3\times 3} & -I_{3\times 3} \\ 0_{3\times 3} & 0_{3\times 3} \\ 0_{3\times 3} & 0_{3\times 3} \end{bmatrix} \tag{33}$$

$$\hat{S}_{w}=diag\left(S_{a,rso},\sigma_{n,gyro}^{2},\frac{2\sigma_{\alpha,ss}^{2}}{\tau_{\alpha}},\frac{2\sigma_{b,gyro,ss}^{2}}{\tau_{gyro}}I_{3\times 3},\frac{2\sigma_{b,los,ss}^{2}}{\tau_{los}}I_{2\times 2},\frac{2\sigma_{b,star,ss}^{2}}{\tau_{star}}I_{3\times 3}\right) \tag{34}$$

REFERENCES

[1] J. Schmidt and T. Lovell, "Estimating Geometric Aspects of Relative Satellite Motion Using Angles-Only Measurements," *Guidance, Navigation, and Control and Co-located Conferences*, pp. –, American Institute of Aeronautics and Astronautics, Aug. 2008, 10.2514/6.2008-6604.

[2] H. Patel, T. A. Lovell, R. Russell, and A. Sinclair, "Relative Navigation for Satellites in Close Proximity Using Angles-Only Observations," *AAS/AIAA Space Flight Mechanics Meeting*, 2012, pp. 12–202.

[3] D. Woffinden and D. Geller, "Observability Criteria for Angles-Only Navigation," *Aerospace and Electronic Systems, IEEE Transactions on*, Vol. 45, No. 3, 2009, pp. 1194–1208, 10.1109/TAES.2009.5259193.

[4] W. H. Clohessy and R. Wiltshire, "Terminal Guidance System for Satellite Rendezvous," *Journal of the Aero/Space Sciences*, Vol. 27, No. 3, 1960, pp. 653–658.

[5] M. L. Psiaki, "Autonomous Orbit Determination for Two Spacecraft from Relative Position Measurements," *Journal of Guidance, Control, and Dynamics*, Vol. 22, Mar. 1999, pp. 305–312, 10.2514/2.4379.

[6] Q. Li, F. Guo, Y. Zhou, and W. Jiang, "Observability of Satellite to Satellite Passive Tracking from Angles Measurements," *Control and Automation, 2007. ICCA 2007. IEEE International Conference on*, 2007, pp. 1926–1931, 10.1109/ICCA.2007.4376697.

[7] J. Schmidt, D. Geller, and F. Chavez, "Viability of Angles-only Navigation for Orbital Rendezvous Operation," *Guidance, Navigation, and Control and Co-located Conferences*, pp. –, American Institute of Aeronautics and Astronautics, Aug. 2010, 10.2514/6.2010-7755.

[8] R. Gillis and D. Geller, "Proximity Operations Using Low Thrust Propulsion an Angles-Only Measurements in Geosynchronous Orbits," *AAS Annual Guidance and Control Conference*, Breckenridge, CO, AAS, 2011.

[9] R. Chari, D. Geller, H. Norris, C. DSouza, and T. Brand, "Autonomous Orbital Rendezvous Using Angles-Only Navigation," *AAS/AIAA Astrodynamics Specialists Conference,*, The Charles Stark Draper Laboratory, 2001.

[10] D. C. Woffinden, *Angles-Only Navigation for Autonomous Orbital Redezvous*. Dissertation, Utah Sate University, dec 2008.

[11] I. Klein and D. Geller, "Zero Delta-V Solution to the Angles-Only Range Observability Problem During Orbital Proximity Operations," *Itzhack Y. Bar-Itzhack Memorial Symposium*, Haifa, Israel, 2012.

[12] P. S. Maybeck, *Stochastic Models, Estimation, and Control*, Vol. 1. New York: Navtech Book and Software Store, 1994.

[13] P. G. Savage, *Strapdown Analytics*. Strapdown Associates, Inc, 2000.